Check for updates

Original Research Article

Spermidine Attenuates Sepsis-associated Acute Lung Injury by Targeting Macrophage Apoptosis via PI3K/Akt Signaling Axis

Pharmacognosy Magazine
22(4) 1438–1448, 2026
© The Author(s) 2026
Article reuse guidelines:
in.sagepub.com/journals-permissions-india
DOI: 10.1177/09731296261417098
journals.sagepub.com/home/phm

Pengcheng Shen[1], Ying Lan[2] and Zhe Bai[3]

Abstract

Background: Sepsis-associated acute lung injury (SALI) is characterized by an uncontrolled inflammatory response and cell apoptosis, with macrophage apoptosis playing a key role in alveolar barrier disruption. Spermidine (SP), as a natural polyamine, has shown potential in anti-aging and immune regulation, but its intervention effect and mechanism on macrophage apoptosis in SALI are not yet clear.

Objectives: This study aimed to investigate the interventional effect of SP on macrophage apoptosis in SALI and to elucidate its potential molecular mechanism.

Materials and Methods: A mouse SALI model was constructed by cecal ligation, and the intervention was performed by intraperitoneal administration of SP. Observe the phenotype of lung injury in SALI mice and the release of pro-inflammatory cytokines. Mechanistically, network pharmacology analysis was used to determine the potential mechanism of SP treatment for SALI and conduct experimental validation.

Results: The results showed that SP treatment significantly reduced the wet-to-dry ratio of lung tissue and the amount of protein exudation in bronchoalveolar lavage fluid, inhibiting the release of pro-inflammatory factors interleukin-1β (IL-1β), interleukin-6 (IL-6), and tumor necrosis factor-α (TNF-α), and alleviating alveolar structural damage. Mechanistically, we employed network pharmacology analysis to indicate that the key mechanism of SP's therapeutic effect on SALI lies in its anti-apoptotic properties. Immunoblot analysis further showed that SP treatment reduced the expression of pro-apoptotic proteins cleaved-caspase 9/3, and Bax in lung tissue, while upregulating the anti-apoptotic protein Bcl-2.

Conclusion: This study elucidates for the first time the mechanism by which SP alleviates SALI by targeting the macrophage apoptosis pathway, providing experimental evidence for the development of lung protection strategies based on immune metabolism regulation.

Keywords

Spermidine, sepsis-associated acute lung injury, apoptosis, network pharmacology, macrophage

Received 07 April 2025; **revised** 29 August 2025; **accepted** 28 November 2025

Introduction

Sepsis-associated acute lung injury (SALI) is a critical condition characterized by an uncontrolled inflammatory response, destruction of the alveolar-capillary barrier, and progressive respiratory failure (Wu et al., 2024; Zhang et al., 2022). In severe cases, it can progress to acute respiratory distress syndrome (ARDS) and become the main cause of death in sepsis patients (Qu et al., 2022). Pathogen-associated molecular patterns (PAMPs), such as lipopolysaccharides (LPS) released by Gram-negative bacteria, are the core factors triggering SALI (Burdette et al., 2021). Despite the use of supportive treatments such as mechanical ventilation, antibiotics, and fluid resuscitation in clinical practice, the mortality rate of SALI is still as high as 30%–40% (Bellani et al., 2016; Nova et al., 2023). Of particular note is that macrophages, as the "hub" of the innate immune response, undergo abnormal apoptosis, which not only exacerbates the breakdown of the alveolar barrier but also forms an "inflammation apoptosis"

[1]Department of Intensive Care Medicine, Yibin First People's Hospital, Yibin, Sichuan, China
[2]Department of Intensive Care Medicine, Chengdu University Affiliated Hospital, Chengdu, Sichuan, China
[3]Department of Cardiology, Bishan Hospital, Chongqing University of Chinese Medicine, Chongqing, China

Corresponding authors:
Ying Lan, Department of Intensive Care Medicine, Chengdu University Affiliated Hospital, Chengdu, Sichuan 610081, China.
E-mail: lanying447431766@163.com
Zhe Bai, Department of Cardiology, Bishan Hospital, Chongqing University of Chinese Medicine, Chongqing 400021, China.
E-mail: 346116215@qq.com

Creative Commons Non Commercial CC BY-NC: This article is distributed under the terms of the Creative Commons Attribution-NonCommercial 4.0 License (http://www.creativecommons.org/licenses/by-nc/4.0/) which permits non-Commercial use, reproduction and distribution of the work without further permission provided the original work is attributed as specified on the SAGE and Open Access pages (https://us.sagepub.com/en-us/nam/open-access-at-sage).

vicious cycle by releasing damage-associated molecular patterns (DAMPs) (Hao et al., 2017).

As a conserved endogenous polyamine in eukaryotes, spermidine (SP) plays multidimensional biological functions in regulating cellular homeostasis (Chamoto et al., 2024). Its metabolic network contains dual sources: the endogenous pathway uses arginine as a precursor, which is catalyzed by ornithine decarboxylase (ODC) to produce putrescine and ultimately synthesize spermine (Chamoto et al., 2024; Zou et al., 2022). The exogenous pathway is absorbed through the enterohepatic circulation through dietary supplementation (such as wheat germ, soybeans, and so on) and gut microbiota metabolism (such as *Pseudomonas aeruginosa* producing SP) (Felgner et al., 2020; Madeo et al., 2018). At the molecular level, SP participates in the regulation of life activities through the following mechanisms: (a) as an autophagy inducer, it activates mitochondrial autophagy through acetylation modification dependent pathways (Jang et al., 2024); (b) as a nucleic acid structure stabilizer, it regulates chromatin condensation and gene transcription (Zhao et al., 2023); (c) as a metabolic regulatory hub, it affects the mechanistic target of rapamycin (mTOR) signaling pathway and polyamine metabolic cycle (Fritsch et al., 2023; Hofer et al., 2024). These characteristics endow SP with broad therapeutic potential, including the delay of aging, improvement of cognitive impairment, inhibition of tumor metastasis, and regulation of cardiovascular metabolism (Chamoto et al., 2024; Eisenberg et al., 2016; Kang et al., 2021; Nie et al., 2023; Zou et al., 2022). It is worth noting that although SP exhibits cardioprotective effects in ischemia–reperfusion injury and hypertension models (Lemay et al., 2024; Liu et al., 2024), there are still key scientific blind spots in its molecular mechanism in SALI.

Based on the known biological functions and protective effects of SP in various physiological systems, it can be reasonably assumed that SP may play a therapeutic role in alleviating SALI. In this case, it is necessary to further investigate the specific mechanism and role of SP, which may lead to the development of new treatment strategies to alleviate SALI and improve the overall quality of life of intensive care unit patients.

Materials and Methods

Reagents

SP (HY-B1776) and (LPS, HY-D1056) were obtained from MedChemExpress. Enzyme-linked immunosorbent assay (ELISA) kits for interleukin-1β (IL-1β, EK201B), interleukin-6 (IL-6, EK206), and tumor necrosis factor-α (TNF-α, EK282HS) were sourced from Hangzhou Lianke Biotechnology Co., Ltd., antibodies against PI3K (60225-1-Ig), AKT (10176-2-AP), phosphorylated AKT (p-AKT, 66444-1-Ig), Bax (50599-2-Ig), Bcl-2 (26593-1-AP), caspase-9 (10380-1-AP), caspase-3 (19677-1-AP), and glyceraldehyde-3-phosphate dehydrogenase (GAPDH) (10494-1-AP) were purchased from Wuhan Proteintech Biotechnology Co., Ltd. (Wuhan, China). The phosphorylated PI3K (p-PI3K, #4228) antibody was obtained from Cell Signaling Technology.

Animal

The establishment plan of the SALI mouse model refers to relevant literature (Qu et al., 2022). Male C57BL/6 mice (6–8 weeks, 18–22 g) were obtained from Beijing Vital River Laboratory Animal Technology Co., Ltd. Animals were housed under standard conditions (22°C, 12/12 h light/dark cycle, ventilation) with free access to food and water. Body weight and food intake were monitored weekly.

Steps for Inducing SALI Model by Cecal Ligation and Puncture (CLP) in Mice

After 6–8 h of fasting, mice underwent isoflurane anesthesia (4% induction, 2% maintenance). The abdomen was shaved, disinfected with iodine, and a midline incision (1.5 cm) was made to expose the cecum. The distal half of the cecum was ligated and punctured twice with a 21-G needle (1 mL volume). Gentle cecal compression allowed minimal intestinal contents leakage into the peritoneal cavity. Sham-operated mice received abdominal incisions without ligation or puncture. Postoperative procedures included layered suturing, iodine disinfection, and subcutaneous injection of 1 mL prewarmed saline to prevent dehydration. Animals were euthanized 48 h post-surgery for model validation.

Animal Group

Mice were randomly divided into four experimental groups:

1. Sham-operated group: Received phosphate-buffered saline (PBS) (intraperitoneal injection, i.p.) followed by sham surgery;
2. SP control group: Administered SP (50 mg/kg, i.p.) with sham surgery;
3. CLP group: Treated with PBS (i.p.) and was subjected to CLP induction;
4. SP + CLP group: Received SP (50 mg/kg, i.p.) and was subjected to CLP induction.

The SP dosing regimen was optimized based on empirical evidence from preclinical studies, with intraperitoneal injection selected over oral administration to ensure precise pharmacokinetic control (Eisenberg et al., 2016; Lifsey et al., 2020).

Lung and Serum Sample Collection

Blood samples (0.5 mL) were collected from the retro-orbital plexus and centrifuged (300 × *g*, 20 min, 4°C) to isolate serum. Mice were then euthanized, and lung tissues were harvested via thoracotomy under sterile conditions for downstream analyses.

Histopathological Examinations

Lung tissues were fixed in 4% paraformaldehyde (24 h), dehydrated through an ethanol gradient, paraffin-embedded, and sectioned into 5 μm slices. Sections were stained with hematoxylin and eosin (H&E) for 2 h according to the manufacturer's protocol and analyzed under a light microscope.

Serum Biochemical Markers

Serum levels of IL-1β, IL-6, and TNF-α were quantified using commercial ELISA kits according to the manufacturers' protocols, with absorbance measured at 450 nm using a microplate reader.

Network Pharmacology

Potential Target Prediction of SP and SALI

Potential targets related to SP were identified through the following databases:

HIT (herbal ingredients' targets, http://www.bad-cao.net:2345/search), Search Tool for Interacting Chemicals (STITCH) (http://stitch.embl.de/), GeneCards (https://www.genecards.org/), Chemical Database of Bioactive Molecules with Drug-like Properties (ChEMBL) (https://www.ebi.ac.uk/chembl/), SEA (similarity ensemble approach, https://sea.bkslab.org/).

For SALI or sepsis, targets were explored using:

GeneCards (https://www.genecards.org/), OMIM (Online Mendelian Inheritance in Man, https://www.omim.org/), DisGeNET (https://disgenet.com), ETCM (Encyclopedia of Traditional Chinese Medicine, http://www.tcmip.cn/ETCM/), TTD (Therapeutic Target Database, http://db.idrblab.net/ttd/).

Potential and Core Targets of SP Therapy for SALI

The core therapeutic targets for SP in SALI were identified by intersecting SP-related targets with SALI-associated genes. Gene interactions among overlapping targets were analyzed via the Search Tool for the Retrieval of Interacting Genes/Proteins (STRING) database (https://cn.string-db.org/) to construct a protein–protein interaction (PPI) network. Hub targets were subsequently prioritized using Cytoscape (v3.9.1) based on topological parameters such as degree centrality and betweenness.

Molecular Docking

The ligand-target interaction profiling implemented a multi-algorithmic docking workflow: (a) Molecular visualization via PyMOL (v2.5.2), (b) automated docking simulations using AutoDockTools (v1.5.7) with the Lamarckian genetic algorithm, and (c) binding pose optimization through OBGUI's (v3.0) force field parameterization. Top-decile target complexes were quantitatively assessed using hybrid scoring metrics incorporating binding free energy (ΔG, kcal/mol), residue-specific interaction fingerprints, and hydrogen-bonding topology matrices to establish a binding hierarchy.

Enrichment Analysis

Core targets underwent Kyoto Encyclopedia of Genes and Genomes (KEGG), gene ontology (GO), and Metascape (https://metascape.org/gp/) enrichment analyzes using Database for Annotation, Visualization and Integrated Discovery (DAVID) (https://david.ncifcrf.gov/). Functional annotations and pathway associations were comprehensively visualized via the bioinformatics platform (https://www.bioinformatics.com.cn/) to elucidate biological mechanisms.

Western Blot

Cryopreserved lung specimens were mechanically disrupted in phenylmethylsulfonyl fluoride (PMSF)-supplemented radioimmunoprecipitation assay (RIPA) lysis buffer (4°C, 60 min). Centrifugation-clarified lysates (12,000 rpm, 15 min, 4°C) were subjected to a bicinchoninic acid (BCA) protein assay (Thermo Fisher Scientific) prior to boiling in Laemmli buffer (10 min, 100°C). Electrophoretic separation employed 12% polyacrylamide gels under denaturing conditions, followed by semi-dry transfer to polyvinylidene difluoride (PVDF) membranes. The immunoblotting protocol included: 5% bovine serum albumin (BSA) blocking, primary antibody incubation (16 h, 4°C), and species-specific immunoglobulin G (IgG)-horseradish peroxidase (HRP) probing (2 h, 22°C). Chemiluminescent signals (BeyoECL Plus) were captured and quantified using a calibrated imaging system (Bio-Rad ImageLab), normalized to the GAPDH housekeeping protein.

Reverse Transcription–Quantitative Polymerase Chain Reaction (RT-qPCR)

The molecular analysis pipeline comprised three phases: (a) Total ribonucleic acid (RNA) isolation using TRIzol reagent (Wuhan Saiweier Biotechnology), (b) complementary DNA (cDNA) synthesis with PrimeScript RT Kit (Tahyperosidera Bio), and (c) SYBR Green qPCR amplification (Tahyperosidera Bio) under optimized cycling conditions (95°C/10 min; 40 × [95°C/15 s → 60°C/30 s]). Relative messenger RNA (mRNA) levels were determined by $2^{-\Delta\Delta CT}$ normalization to β-actin, using custom-designed primers (Sangon Biotech) specified in Table 1.

Statistical Analysis

The data are displayed as mean ± standard error of the mean (SEM). Prior to conducting parametric analyzes, the data distribution normality and variance homogeneity were verified using both one-way and two-way analysis of variance

(ANOVA) frameworks. Significant between-group differences were subsequently analyzed through Tukey's honestly significant difference (HSD) procedure, with statistical significance determined at $p < .05$.

Table 1. Sequences of the Primers Used in the Polymerase Chain Reaction (PCR) Measurement.

Gene	Sense	Sequence (5′ to 3′)
TNFα	TNFα-FWD	CCGATGGGTTGTACCTTGTC
	TNFα-REV	GGGCTGGGTAGAGAATGGAT
IL-1β	IL-1β-FWD	CCAGCTTCAAATCTCACAGCAG
	IL-1β-REV	CTTCTTTGGGTATTGCTTGGGATC
IL-6	IL-6-FWD	TCCTACCCCAATTTCCAATGC
	IL-6-REV	CATAACGCACTAGGTTTGCCG
β-actin	β-actin -FWD	CCACTGCCGCATCCTCTTCCTC
	β-actin-REV	TCCTGCTTGCTGATCCACATCT

Source: All PCR primers were synthesized by Sangen Biotechnology (Shanghai, China).

Results

SP Ameliorates CLP-induced Pulmonary Dysfunction in Mice

As illustrated in Figure 1, CLP surgery induced significant pulmonary pathophysiology compared with the sham group. Specifically, CLP-treated mice exhibited markedly elevated airway resistance (Figure 1A) and lung compliance (Figure 1B), accompanied by increased arterial carbon dioxide tension ($PaCO_2$, Figure 1E) and total carbon dioxide (TCO_2, Figure 1F). Conversely, pulmonary ventilation capacity (Figure 1C) and arterial oxygen tension (PaO_2, Figure 1D) were substantially reduced in the CLP group. Notably, SP administration effectively reversed these CLP-induced alterations, significantly attenuating airway resistance, lung compliance, $PaCO_2$, and TCO_2 levels while restoring pulmonary ventilation and PaO_2 to near-normal ranges (SP + CLP vs. CLP, Figure 1A–1F). Importantly, SP monotherapy in sham-operated mice showed no significant effects on any respiratory parameters (SP +

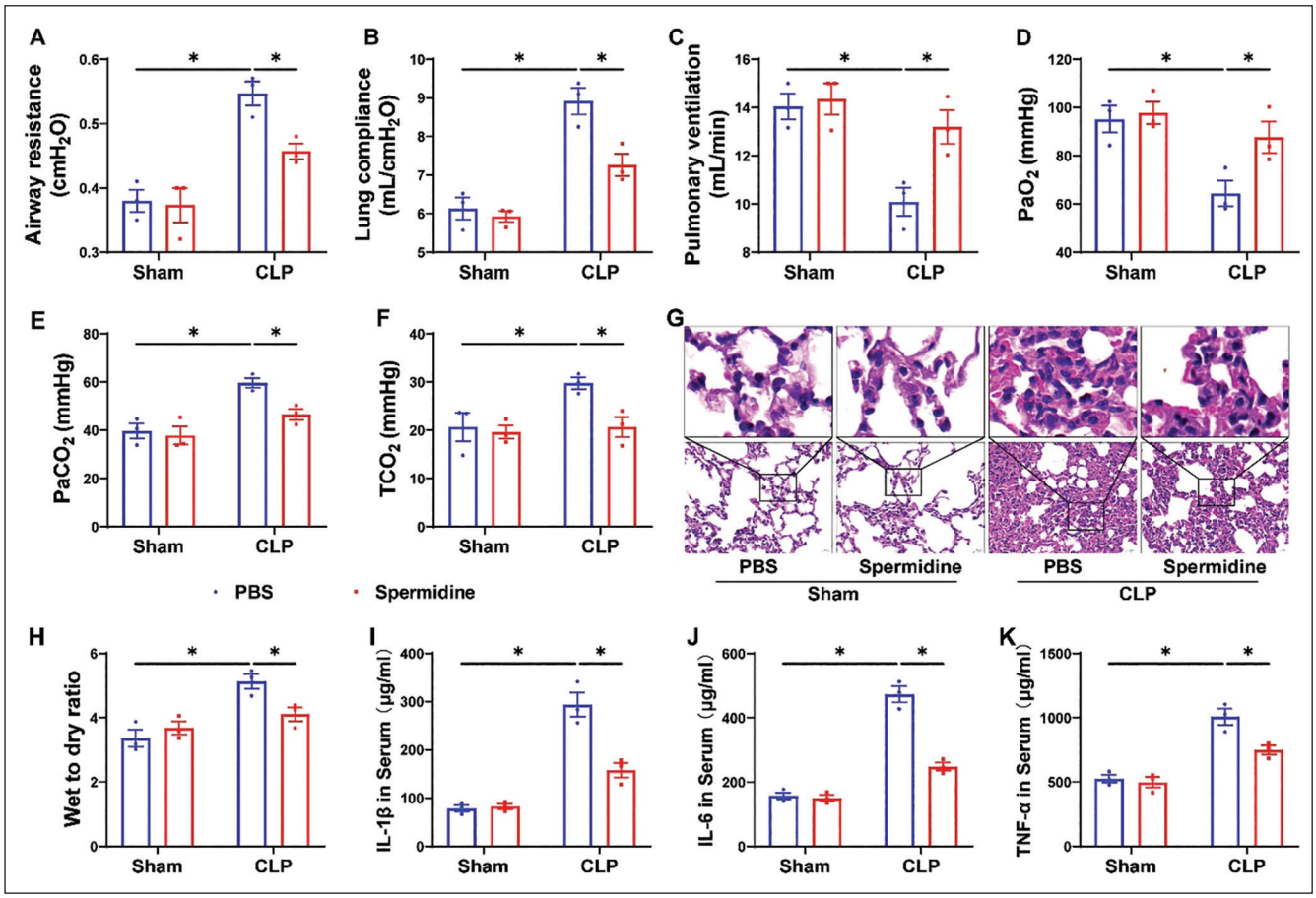


Figure 1. Therapeutic Efficacy of Spermidine in SALI Mice Models. Multiparametric Evaluation Demonstrates: (A and B) Respiratory Mechanics Improvement (Airway Resistance & Lung Compliance). (C) Pulmonary Ventilatory Function Recovery. (D-F) Blood Gas Homeostasis Restoration (PaO_2/$PaCO_2$/TCO_2), (G) Histopathological Attenuation (H&E). (H) Edema Reduction (Wet to Dry Ratio). (I-K) Cytokine Storm Suppression (IL-1β/IL-6/TNF-α).

Note: *$p < .05$.

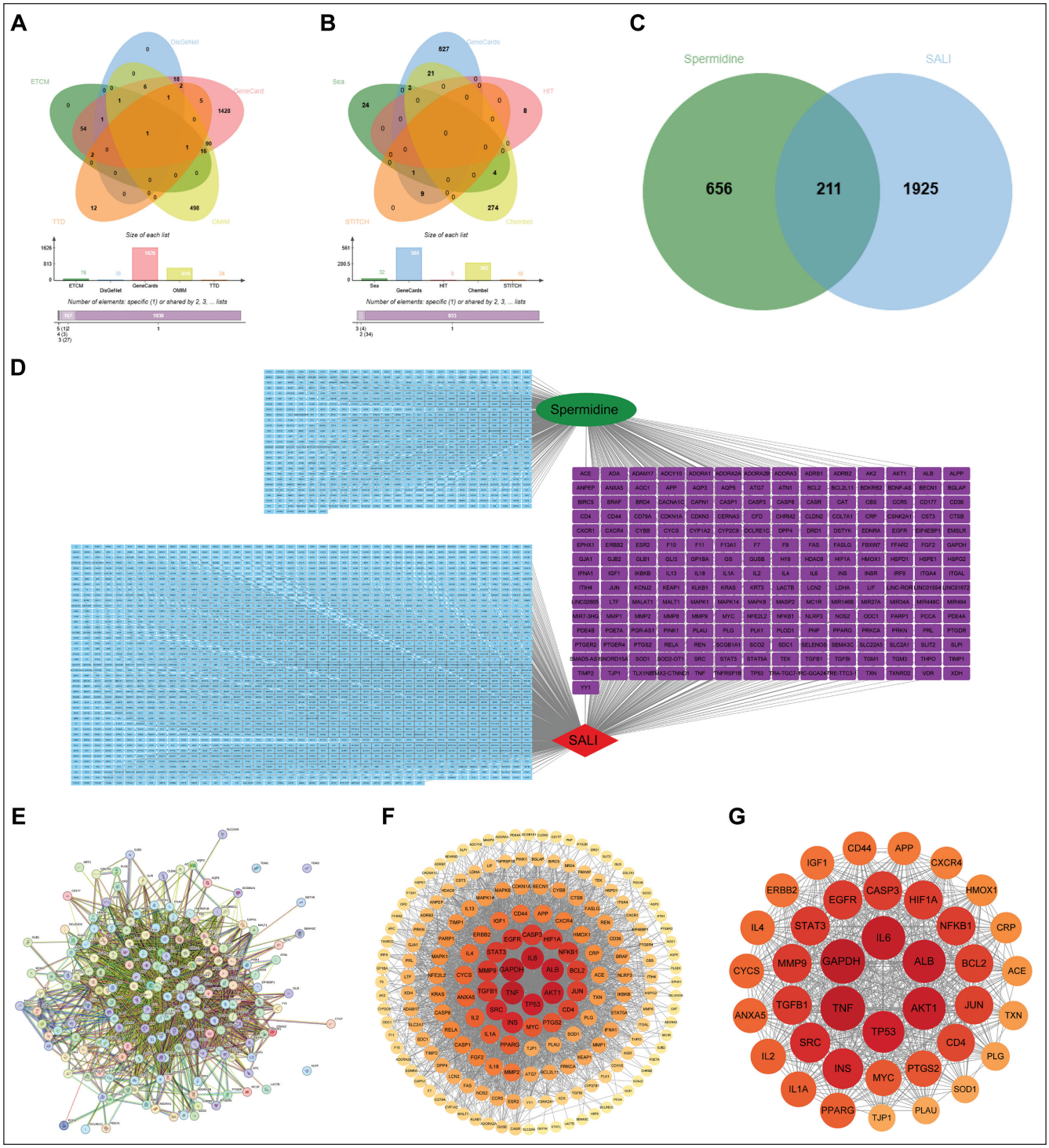


Figure 2. Systems Pharmacology Interrogation of Spermidine's Therapeutic Targets in SALI (A) Target Landscape of SALI Pathogenesis. (B) Spermidine's Pharmacodynamic Targets. (C) Venn Intersection Analysis Identifying 211 Shared Targets. (D) Protein-protein Interaction (PPI) Network of Consensus Targets (STRING). (E) Network Topology Interrogation Using CytoHubba Algorithms, Ranking of (F) Potential Targets and (G) Core Targets. Node Size Correlates with Topological Significance.

Sham vs. Sham, Figure 1A–1F), confirming its therapeutic safety under non-pathological conditions.

Histopathological analysis further corroborated these findings (Figure 1G and 1H). CLP-induced lung injury was characterized by alveolar septal thickening, pronounced capillary congestion, perivascular inflammatory cell infiltration, and increased dry-to-wet weight ratio of lung tissue (CLP vs. Sham). SP treatment substantially ameliorated these pathological

alterations (SP + CLP vs. CLP), demonstrating preserved alveolar architecture and reduced inflammatory markers in the SP + CLP group. No discernible histopathological changes were observed in SP-treated sham controls, consistent with the functional parameter observations (SP + Sham vs. Sham).

SP Attenuates CLP-induced Systemic Inflammation in Mice

As demonstrated in Figure 1I–1K, CLP surgery triggered a pronounced systemic inflammatory response compared to sham-operated controls. Serum levels of pro-inflammatory cytokines, IL-1β (Figure 1I), IL-6 (Figure 1J), and TNF-α (Figure 1K), were significantly elevated in CLP mice (CLP vs. Sham). Remarkably, SP administration markedly suppressed CLP-induced hyperinflammation, as evidenced by reduced serum concentrations of IL-1β, IL-6, and TNF-α (SP + CLP vs. CLP, Figure 1I–1K). Importantly, SP monotherapy in sham-operated mice did not alter baseline levels of these inflammatory mediators (SP + Sham vs. Sham, Figure 1I–1K),

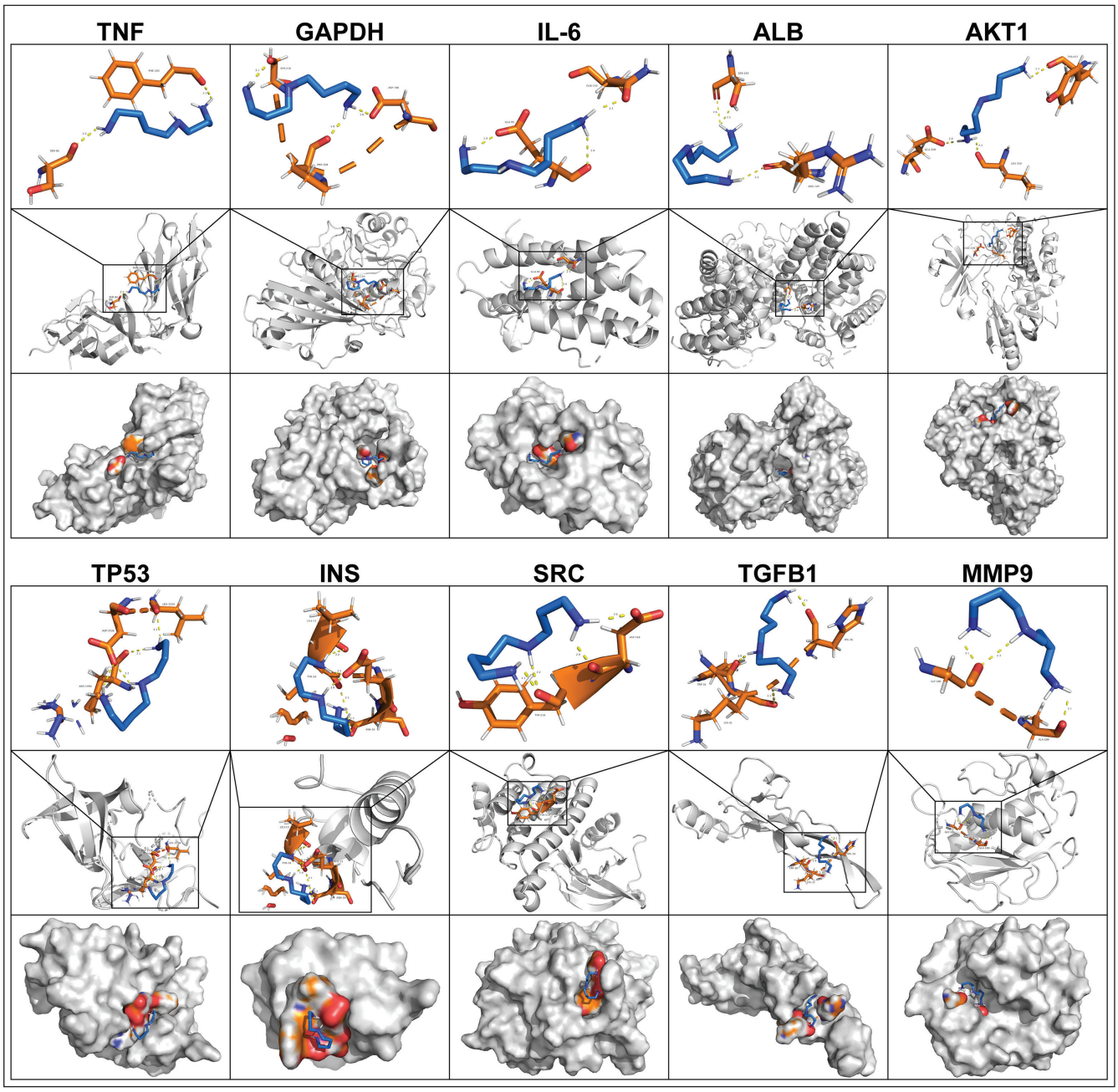


Figure 3. Details of Molecular Docking Between Spermidine and the Top Ten Core Targets. Visualization of Molecular Docking Between Spermidine and the Top Ten Core Targets, Including TNF (5M2J), GAPDH (4WNC), IL-6 (1ALU), ALB (7DJN), AKT1 (6EJN), TP53 (6VA5), INS (3I40), SRC (2BDJ), TGFB1 (1KLD), and MMP9 (6ESM).

underscoring its selective anti-inflammatory efficacy under pathological conditions.

Network Pharmacology Reveals SP's Potential Targets in SALI

To systematically investigate SP's therapeutic mechanism against SALI, we performed a comprehensive network pharmacology analysis. As illustrated in Figure 2A, 2,136 SALI-related therapeutic targets were compiled from five disease databases: ETCM (76 targets), DisGeNet (30), GeneCards (1,626), OMIM (614), and TTD (24). Concurrently, 867 SP-associated targets were identified across five pharmacological databases (Figure 2B): SEA (13), GeneCards (561), HIT (8), ChEMBL (302), and STITCH (10). Intersection analysis revealed 211 overlapping targets (Figure 2C), representing potential key mediators of SP's therapeutic effects in SALI.

The target network was visualized using Cytoscape (Figure 2D), followed by STRING database analysis to map PPI among the 211 shared targets (Figure 2E). Target prioritization was conducted via the CentiScaPe 2.2 plugin, with node darkness proportional to topological importance (Figure 2F). Further refinement identified the core therapeutic targets through centrality analysis (Figure 2G), highlighting critical nodes in SP's SALI-modulatory network.

Molecular Docking Analysis Reveals SP's Interactions with Core SALI Targets

Molecular docking simulations were performed to evaluate the binding interactions between SP and the top 10 prioritized core targets identified in SALI pathogenesis. As illustrated in Figure 3, SP exhibited stable binding conformations with all targets, with binding affinities (docking scores) and hydrogen bond interactions detailed in Table 2. Notably, SP demonstrated strong binding to MMP9, TP53, and INS, suggesting these as potential key mediators of its therapeutic effects. Intermediate affinity was observed for TNF, GAPDH, and SRC, while IL-6 exhibited the weakest interaction. ALB, AKT1, and TGFB1 displayed moderate binding with distinct hydrogen bonding patterns.

Functional Enrichment Analysis Highlights SP's Mechanistic Pathways in SALI

To delineate the therapeutic mechanisms of SP in SALI, functional enrichment analysis was performed on the 211 overlapping targets. GO analysis (Figure 4A) revealed significant enrichment in biological processes critical to SALI pathogenesis, notably "negative regulation of apoptosis" and "inflammatory response," underscoring SP's dual role in modulating cell survival and immune homeostasis. KEGG

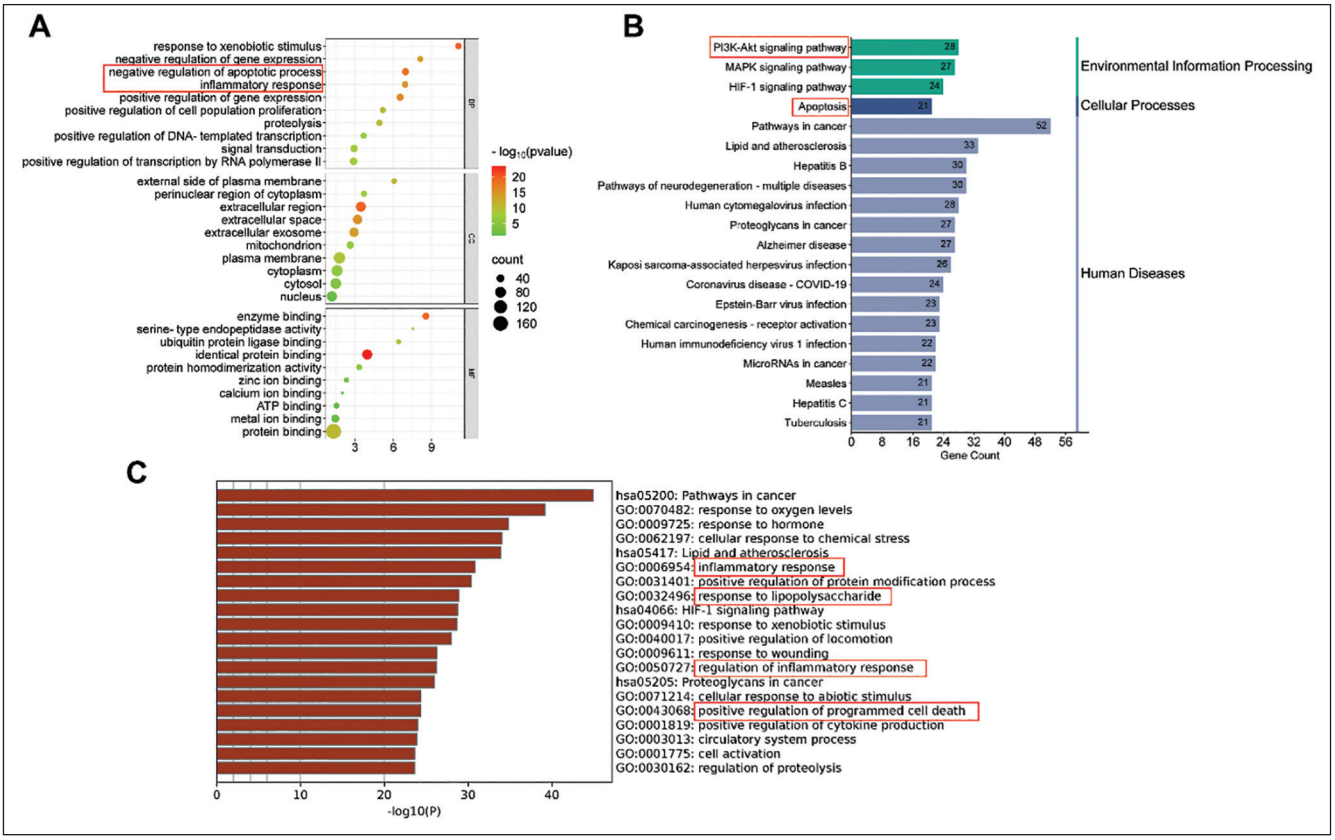


Figure 4. Enrichment Analysis in Network Pharmacology. GO Analysis (A), Metescape Analysis (B), and KEGG (C) Analysis of Potential Therapeutic Targets.

Table 2. Details of Molecular Docking Between Spermidine (SP) and the Top 10 Core Targets.

Drug	Target	PDB ID	Binding Energy	Hydrogen Bonds
Spermidine	TNF	5M2J	−2.48	3
	GAPDH	4WNC	−2.68	3
	IL-6	1ALU	−1.43	2
	ALB	7DJN	−1.96	1
	AKT1	6EJN	−2.4	1
	TP53	6VA5	−3.07	1
	INS	3I40	−2.82	3
	SRC	2BDJ	−2.29	3
	TGFB1	1KLD	−2.91	1
	MMP9	6ESM	−3.31	3

Notes: The binding energy and number of hydrogen bonds between SP and the top 10 core targets. GAPDH: Glyceraldehyde-3-phosphate dehydrogenase; IL-6: Interleukin-6; TNF: tumor necrosis factor.

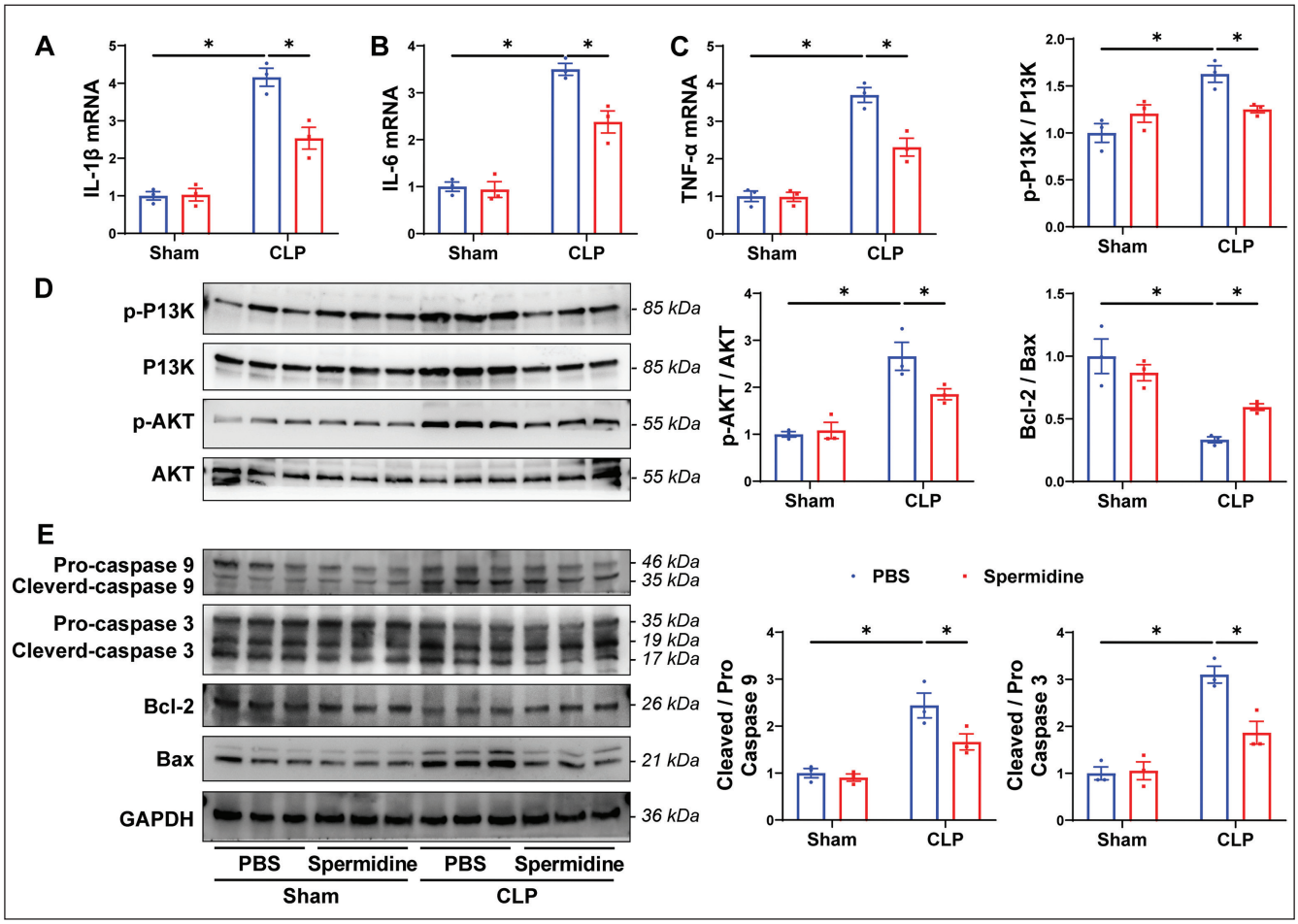


Figure 5. Inflammatory and Apoptotic Modulation of Spermidine in BALF Macrophages. Changes in Inflammation Related Genes IL-1 (A), IL-6 (B), and TNF (C) in BALF Macrophages. Changes in the Levels of P13K-Akt Signaling Pathway (D) in BALF Macrophages. Changes in Apoptosis Related Protein Levels Cleaved-Caspase-9/3 and Bax/Bcl-2 Ratios in BALF Macrophages (E).

Note: *$p < .05$.

pathway analysis (Figure 4B) prioritized the "PI3K/Akt signaling pathway" and "apoptosis" as central pathways modulated by SP, suggesting its potential to attenuate hyperinflammatory cascades and apoptotic cell death in SALI. Metascape analysis (Figure 4 C) further corroborated these findings, identifying "inflammation response," "regulation of inflammatory response," "response to LPS," and "positive regulation of programmed cell death" as robustly enriched pathways, aligning with sepsis-driven lung injury mechanisms.

SP Modulates PI3K/Akt Signaling, Inflammation, and Apoptosis in Macrophages During SALI

Guided by network pharmacology predictions implicating apoptosis and inflammation as pivotal mechanisms, we investigated SP's effects on macrophage pathophysiology in SALI. CLP surgery significantly upregulated pro-inflammatory cytokine mRNA levels (IL-1β, IL-6, and TNF-α) in lung tissue macrophages compared to sham controls (Figure 5A–5C). SP treatment robustly attenuated these CLP-induced inflammatory surges (SP + CLP vs. CLP), restoring cytokine expression to near-baseline levels. CLP triggered hyperactivation of the PI3K/Akt pathway (Figure 5D) and elevated apoptotic markers, including cleaved-caspase-9/3 ratios and the Bax/Bcl-2 imbalance (Figure 5E). SP administration suppressed both PI3K/Akt signaling and apoptosis-related protein dysregulation (SP + CLP vs. CLP, Figure 5D), demonstrating its dual regulatory capacity. Notably, SP monotherapy in sham-operated mice exerted no significant effects on inflammatory cytokines, PI3K/Akt activity, or apoptotic markers (SP + Sham vs. Sham, Figure 5A–5E), confirming its context-dependent efficacy and safety in non-pathological states.

Discussion

The anti-inflammatory properties of SP observed here align with prior reports of its immunomodulatory effects in aging and metabolic disorders (Guarente et al., 2024; Zhang et al., 2023). However, this study uniquely demonstrates its capacity to disrupt the "inflammation-apoptosis" vicious cycle in SALI. By suppressing CLP-induced hyperactivation of PI3K/Akt signaling, SP attenuated both macrophage apoptosis (via Bax/Bcl-2 balance restoration and caspase-9/3 cleavage inhibition) and the cytokine storms (IL-1β, IL-6, TNF-α). This dual mechanism is particularly significant, as PI3K/Akt serves as a convergence point for survival signaling and inflammatory crosstalk (Salvadori et al., 2021; Shen et al., 2024). Our network pharmacology and molecular docking analyzes further rationalize these effects, identifying high-affinity interactions between SP and apoptosis- and inflammation-regulating proteins (e.g., TP53, MMP9, TNF), which may synergistically amplify its therapeutic impact. The enrichment of "response to LPS" in Metascape analysis underscores SP's relevance to Gram-negative sepsis, the primary SALI etiology (Kumar, 2020). By mitigating LPS-driven TLR4 signaling downstream events (e.g., NETosis, cytokine release), SP may complement antibiotic therapies that fail to address post-infectious immune dysregulation (Espinoza-Culupú et al., 2020; Ma et al., 2020; Xu et al., 2024). This positions SP as a potential adjuvant therapy to break the "double-hit" paradigm of SALI-direct pathogen toxicity followed by host-derived collateral damage.

Mechanistically, SP's ability to stabilize Bcl-2 and suppress caspases may involve direct binding (as predicted by docking) or indirect epigenetic regulation via chromatin modulation, a known polyamine function warranting further exploration. But the regulation of the PI3K/AKT pathway by SP is currently unclear. However, in this study, the molecular docking binding energy between SP and Akt was low, suggesting that the possibility of regulating the P13K/Akt pathway through direct binding is unlikely. In addition, the literature suggests that SP is closely related to epigenetic reprogramming (histone hyperacetylation and deoxyribonucleic acid (DNA) methylation switching) and the autophagy feedback loop, and we have reason to suspect that this may be its potential pathway of action (Guarente et al., 2024; Liang et al., 2020). SP selectively regulates macrophage apoptosis rather than other immune cells (such as neutrophils), and is closely related to its unique autophagy induction function (Liu et al., 2020; Pietrocola et al., 2015; Yuan et al., 2025; Zhang et al., 2019). Our findings bridge critical knowledge gaps in polyamine biology and sepsis immunopathology, offering novel insights into SP's role as a multitarget modulator of immune cell fate and inflammatory homeostasis.

Limitations

Despite these advances, limitations exist. First, while CLP models replicate human sepsis pathophysiology, interspecies differences in polyamine metabolism (e.g., gut microbiota-dependent SP synthesis) necessitate validation in human macrophages or organoids. Second, the 50 mg/kg dosage—though effective here—requires pharmacokinetic optimization to balance efficacy with potential polyamine toxicity at supraphysiological levels. Third, the precise hierarchy among the 211 identified targets remains unclear; clustered regularly interspaced short palindromic repeats (CRISPR)-based screening could delineate indispensable nodes in SP's SALI-modulatory network. Through interdisciplinary technology integration (nanotechnology + synthetic biology + microbiology), a species universal SP delivery platform can be constructed, providing breakthrough treatment options for sepsis-related immune disorders such as acute lung injury.

Conclusion

In conclusion, this work establishes SP as a promising immunometabolic therapeutic for SALI, leveraging its evolutionarily conserved roles in stress adaptation. By decoupling

inflammation from apoptosis in macrophages, SP offers a blueprint for developing pathophysiology-responsive therapies in critical care medicine.

Acknowledgments

This study does not involve any clinical trials or human samples.

Declaration of Conflicting Interests

The authors declared no potential conflicts of interest with respect to the research, authorship, and/or publication of this article.

Ethical Approval and Informed Consent

The experimental protocol was approved by the Research Ethics Committee of Chengdu University Affiliated Hospital.

Funding

The authors disclosed receipt of the following financial support for the research, authorship, and/or publication of this article: This project was supported by the Chongqing Natural Science Foundation General Project of China (CSTB2022NSCQ-MSX1490).

ORCID iD

Zhe Bai https://orcid.org/0009-0001-0424-4251

References

Bellani, G., Laffey, J. G., Pham, T., Fan, E., Brochard, L., Esteban, A., Gattinoni, L., van Haren, F., Larsson, A., McAuley, D. F., Ranieri, M., Rubenfeld, G., Thompson, B. T., Wrigge, H., Slutsky, A. S., Pesenti, A., LUNG SAFE Investigators, & ESICM Trials Group. (2016). Epidemiology, patterns of care, and mortality for patients with acute respiratory distress syndrome in intensive care units in 50 countries. *JAMA*, *315*(8), 788–800. https://doi.org/10.1001/jama.2016.0291

Burdette, B. E., Esparza, A. N., Zhu, H., & Wang, S. (2021). Gasdermin D in pyroptosis. *Acta Pharmaceutica Sinica B*, *11*(9), 2768–2782. https://doi.org/10.1016/j.apsb.2021.02.006

Chamoto, K., Zhang, B., Tajima, M., Honjo, T., & Fagarasan, S. (2024). Spermidine—An old molecule with a new age-defying immune function. *Trends in Cell Biology*, *34*(5), 363–370. https://doi.org/10.1016/j.tcb.2023.08.002

Eisenberg, T., Abdellatif, M., Schroeder, S., Primessnig, U., Stekovic, S., Pendl, T., Harger, A., Schipke, J., Zimmermann, A., Schmidt, A., Tong, M., Ruckenstuhl, C., Dammbrueck, C., Gross, A. S., Herbst, V., Magnes, C., Trausinger, G., Narath, S., Meinitzer, A., … Madeo, F. (2016). Cardioprotection and lifespan extension by the natural polyamine spermidine. *Nature Medicine*, *22*(12), 1428–1438. https://doi.org/10.1038/nm.4222

Espinoza-Culupú, A., Vázquez-Ramírez, R., Farfán-López, M., Mendes, E., Notomi Sato, M., da Silva Junior, P. I., & Borges, M. M. (2020). Acylpolyamine mygalin as a TLR4 antagonist based on molecular docking and in vitro analyses. *Biomolecules*, *10*(12). https://doi.org/10.3390/biom10121624

Felgner, S., Preusse, M., Beutling, U., Stahnke, S., Pawar, V., Rohde, M., Brönstrup, M., Stradal, T., & Häussler, S. (2020). Host-induced spermidine production in motile *Pseudomonas aeruginosa* triggers phagocytic uptake. *Elife*, *9*. https://doi.org/10.7554/eLife.55744

Fritsch, S. D., Sukhbaatar, N., Gonzales, K., Sahu, A., Tran, L., Vogel, A., Mazic, M., Wilson, J. L., Forisch, S., Mayr, H., Oberle, R., Weiszmann, J., Brenner, M., Vanhoutte, R., Hofmann, M., Pirnes-Karhu, S., Magnes, C., Kühnast, T., Weckwerth, W., … Weichhart, T. (2023). Metabolic support by macrophages sustains colonic epithelial homeostasis. *Cell Metabolism*, *35*(11), 1931–1943.e1938. https://doi.org/10.1016/j.cmet.2023.09.010

Guarente, L., Sinclair, D. A., & Kroemer, G. (2024). Human trials exploring anti-aging medicines. *Cell Metabolism*, *36*(2), 354–376. https://doi.org/10.1016/j.cmet.2023.12.007

Hao, H., Cao, L., Jiang, C., Che, Y., Zhang, S., Takahashi, S., Wang, G., & Gonzalez, F. J. (2017). Farnesoid X receptor regulation of the NLRP3 inflammasome underlies cholestasis-associated sepsis. *Cell Metabolism*, *25*(4), 856–867.e855. https://doi.org/10.1016/j.cmet.2017.03.007

Hofer, S. J., Daskalaki, I., Abdellatif, M., Stelzl, U., Sedej, S., Tavernarakis, N., Kroemer, G., & Madeo, F. (2024). A surge in endogenous spermidine is essential for rapamycin-induced autophagy and longevity. *Autophagy*, *20*(12), 2824–2826. https://doi.org/10.1080/15548627.2024.2396793

Jang, J. S., Hong, S. J., Mo, S., Kim, M. K., Kim, Y. G., Lee, Y., & Kim, H. H. (2024). PINK1 restrains periodontitis-induced bone loss by preventing osteoclast mitophagy impairment. *Redox Biology*, *69*, 103023. https://doi.org/10.1016/j.redox.2023.103023

Kang, X., Li, C., Xie, Y., He, L. L., Xiao, F., Zhan, K. B., Tang, Y.-Y., Li, X., & Tang, X. Q. (2021). Hippocampal ornithine decarboxylase/spermidine pathway mediates H_2S-alleviated cognitive impairment in diabetic rats: Involving enhancement of hippocampal autophagic flux. *Journal of Advanced Research*, *27*, 31–40. https://doi.org/10.1016/j.jare.2020.06.007

Kumar, V. (2020). Pulmonary innate immune response determines the outcome of inflammation during pneumonia and sepsis-associated acute lung injury. *Frontiers in Immunology*, *11*, 1722. https://doi.org/10.3389/fimmu.2020.01722

Lemay, S. E., Grobs, Y., Romanet, C., Martineau, S., Salem, M., Shimauchi, T., Breuils-Bonnet, S., Bourgeois, A., Théberge, C., Pelletier, A., Potus, F., Provencher, S., Bonnet, S., & Boucherat, O. (2024). Hypusine signaling promotes pulmonary vascular remodeling in pulmonary arterial hypertension. *American Journal of Respiratory and Critical Care Medicine*, *209*(11), 1376–1391. https://doi.org/10.1164/rccm.202305-0909OC

Liang, W., Yamahara, K., Hernando-Erhard, C., Lagies, S., Wanner, N., Liang, H., Schell, C., Kammerer, B., Huber, T. B., & Bork, T. (2020). A reciprocal regulation of spermidine and autophagy in podocytes maintains the filtration barrier. *Kidney International*, *98*(6), 1434–1448. https://doi.org/10.1016/j.kint.2020.06.016

Lifsey, H. C., Kaur, R., Thompson, B. H., Bennett, L., Temel, R. E., & Graf, G. A. (2020). Stigmasterol stimulates transintestinal cholesterol excretion independent of liver X receptor activation in the small intestine. *The Journal of Nutritional Biochemistry*, *76*, 108263. https://doi.org/10.1016/j.jnutbio.2019.108263

Liu, Z., Chen, H., Song, Y., Chen, K., Pan, S., Yang, S., & Lu, D. (2024). Inhibition of Sat1 alleviates myocardial ischemia–reperfusion injury through regulation of ferroptosis via MAPK/ERK pathway. *Frontiers in Pharmacology*, *15*, 1476718. https://doi.org/10.3389/fphar.2024.1476718

Liu, R., Li, X., Ma, H., Yang, Q., Shang, Q., Song, L., Zheng, Z., Zhang, S., Pan, Y., Huang, P., Fang, J., Li, Y., Liu, Z., Cao, L., Feng, C., Gong, Z., Chen, Y., Wang, Y., Melino, G., ... Shi, Y. (2020). Spermidine endows macrophages anti-inflammatory properties by inducing mitochondrial superoxide-dependent AMPK activation, Hif-1α upregulation and autophagy. *Free Radical Biology and Medicine*, *161*, 339–350. https://doi.org/10.1016/j.freeradbiomed.2020.10.029

Ma, L., Ni, Y., Wang, Z., Tu, W., Ni, L., Zhuge, F., Zheng, A., Hu, L., Zhao, Y., Zheng, L., & Fu, Z. (2020). Spermidine improves gut barrier integrity and gut microbiota function in diet-induced obese mice. *Gut Microbes*, *12*(1), 1–19. https://doi.org/10.1080/19490976.2020.1832857

Madeo, F., Eisenberg, T., Pietrocola, F., & Kroemer, G. (2018). Spermidine in health and disease. *Science*, *359*(6374). https://doi.org/10.1126/science.aan2788

Nie, T., Liu, H., Fang, Z., Zheng, Y., Zhang, R., Xu, X., Liu, S., & Wu, J. (2023). Tumor microenvironment mediated spermidine-metal-immunopeptide nanocomplex for boosting ferroptotic immunotherapy of lymphoma. *ACS Nano*, *17*(11), 10925–10937. https://doi.org/10.1021/acsnano.3c02803

Nova, A., Rezoagli, E., Eronia, N., Foti, G., & Bellani, G. (2023). Role of PEEP on the prognostic performance of the ROX index in hypoxemic respiratory failure due to COVID-19: Any further gain in outcome prediction? *Intensive Care Medicine*, *49*(3), 355–356. https://doi.org/10.1007/s00134-022-06965-x

Pietrocola, F., Lachkar, S., Enot, D. P., Niso-Santano, M., Bravo-San Pedro, J. M., Sica, V., Izzo, V., Maiuri, M. C., Madeo, F., Mariño, G., & Kroemer, G. (2015). Spermidine induces autophagy by inhibiting the acetyltransferase EP300. *Cell Death & Differentiation*, *22*(3), 509–516. https://doi.org/10.1038/cdd.2014.215

Qu, M., Chen, Z., Qiu, Z., Nan, K., Wang, Y., Shi, Y., Shao, Y., Zhong, Z., Zhu, S., Guo, K., Chen, W., Lu, X., Wang, Z., Zhang, H., & Miao, C. (2022). Neutrophil extracellular traps-triggered impaired autophagic flux via METTL3 underlies sepsis-associated acute lung injury. *Cell Death Discovery*, *8*(1), 375. https://doi.org/10.1038/s41420-022-01166-3

Salvadori, G., Zanardi, F., Iannelli, F., Lobefaro, R., Vernieri, C., & Longo, V. D. (2021). Fasting-mimicking diet blocks triple-negative breast cancer and cancer stem cell escape. *Cell Metabolism*, *33*(11), 2247–2259.e2246. https://doi.org/10.1016/j.cmet.2021.10.008

Shen, S., Sun, T., Ding, X., Gu, X., Wang, Y., Ma, X., Li, Z., Gao, H., Ge, S., & Feng, Q. (2024). The exoprotein Gbp of *Fusobacterium nucleatum* promotes THP-1 cell lipid deposition by binding to CypA and activating PI3K-AKT/MAPK/NF-κB pathways. *Journal of Advanced Research*, *57*, 93–105. https://doi.org/10.1016/j.jare.2023.04.007

Wu, D., Spencer, C. B., Ortoga, L., Zhang, H., & Miao, C. (2024). Histone lactylation-regulated METTL3 promotes ferroptosis via m6A-modification on ACSL4 in sepsis-associated lung injury. *Redox Biology*, *74*, 103194. https://doi.org/10.1016/j.redox.2024.103194

Xu, H., Zhang, X., Wang, X., Li, B., Yu, H., Quan, Y., Jiang, Y., You, Y., Wang, Y., Wen, M., Liu, J., Wang, M., Zhang, B., Li, Y., Zhang, X., Lu, Q., Yu, C.-Y., & Cao, X. (2024). Cellular spermine targets JAK signaling to restrain cytokine-mediated autoimmunity. *Immunity*, *57*(8), 1796–1811.e1798. https://doi.org/10.1016/j.immuni.2024.05.025

Yuan, X., Mao, Y., Chen, Y., Zhuang, J., Chen, D., & Li, X. (2025). Spermine enhances cholesterol effluence of macrophages through caspase 2-mediated autophagy. *Discovery Medicine*, *37*(196), 884–893. https://doi.org/10.24976/Discov.Med.202537196.78

Zhang, H., Alsaleh, G., Feltham, J., Sun, Y., Napolitano, G., Riffelmacher, T., Charles, P., Frau, L., Hublitz, P., Yu, Z., Mohammed, S., Ballabio, A., Balabanov, S., Mellor, J., & Simon, A. K. (2019). Polyamines control eIF5A hypusination, TFEB translation, and autophagy to reverse B cell senescence. *Molecular Cell*, *76*(1), *110*.e119–125.e119. https://doi.org/10.1016/j.molcel.2019.08.005

Zhang, Y., Bai, J., Cui, Z., Li, Y., Gao, Q., Miao, Y., & Xiong, B. (2023). Polyamine metabolite spermidine rejuvenates oocyte quality by enhancing mitophagy during female reproductive aging. *Nature Aging*, *3*(11), 1372–1386. https://doi.org/10.1038/s43587-023-00498-8

Zhang, H., Liu, J., Zhou, Y., Qu, M., Wang, Y., Guo, K., Shen, R., Sun, Z., Cata, J. P., Yang, S., Chen, W., & Miao, C. (2022). Neutrophil extracellular traps mediate m(6)A modification and regulates sepsis-associated acute lung injury by activating ferroptosis in alveolar epithelial cells. *International Journal of Biological Sciences*, *18*(8), 3337–3357. https://doi.org/10.7150/ijbs.69141

Zhao, C., Ma, Y., Zhang, M., Gao, X., Liang, W., Qin, Y., Fu, Y., Jia, M., Song, H., Gao, C., & Zhao, W. (2023). Polyamine metabolism controls B-to-Z DNA transition to orchestrate DNA sensor cGAS activity. *Immunity*, *56*(11), 2508–2522.e2506. https://doi.org/10.1016/j.immuni.2023.09.012

Zou, D., Zhao, Z., Li, L., Min, Y., Zhang, D., Ji, A., Jiang, C., Wei, X., & Wu, X. (2022). A comprehensive review of spermidine: Safety, health effects, absorption and metabolism, food materials evaluation, physical and chemical processing, and bioprocessing. *Comprehensive Reviews in Food Science and Food Safety*, *21*(3), 2820–2842. https://doi.org/10.1111/1541-4337.12963